

RESEARCH

Open Access



A pyrimidine metabolism-related gene signature for prognosis prediction and immune microenvironment description of breast cancer

Han Wang^{1†}, Ziling Zhou^{1†}, Hanyi Zhong^{1†}, Shoutang Wang³, Kunwei Shen¹, Renhong Huang^{1*}, Ruo Wang^{2*} and Zheng Wang^{1*}

Abstract

Background Metabolic reprogramming is a hallmark in cancer. Pyrimidine metabolism (PM), a part of nucleotide metabolism, has been shown to be associated with the progression of various cancers, and the prognostic predictive ability of pyrimidine metabolism-related genes (PMG) in breast cancer has not been elucidated. This paper was designed to identify pyrimidine metabolism-related prognostic marker of breast cancer and potential targeted therapeutic options.

Methods The cohort in the TCGA-BRCA dataset was used for patient information, and 108 pyrimidine metabolism-related genes were identified from the MSigDB KEGG pathways. We identified PM clusters in breast cancer and established a PM risk score model based on 10 pyrimidine metabolism-related genes. The status of immune infiltration was assessed in different groups. Further we identified the relevant hub gene and analyzed its significance for breast cancer metastasis and explored patterns of combination therapy.

Results We identified three types of PM clusters in breast cancer and clarified that PM cluster C with inferior prognosis possessed activation of tumor proliferation-associated pathways. The high-risk group in PM risk score model was found to be characterized by an immunosuppressive microenvironment. The hub gene POLR2C (RNA polymerase II subunit C) was further identified and verified as a potential prognostic marker. Furthermore, targeting POLR2C in combination with anti-PD-1 and anti-angiogenic therapies demonstrated a promising tumor suppression effect, suggesting a potential therapeutic direction.

[†]Han Wang, Ziling Zhou and Hanyi Zhong contributed equally to this work.

*Correspondence:
Renhong Huang
hrh1217@sjtu.edu.cn
Ruo Wang
wangruo@fzu.edu.cn
Zheng Wang
zhengwangwilson@163.com

Full list of author information is available at the end of the article



© The Author(s) 2025. **Open Access** This article is licensed under a Creative Commons Attribution-NonCommercial-NoDerivatives 4.0 International License, which permits any non-commercial use, sharing, distribution and reproduction in any medium or format, as long as you give appropriate credit to the original author(s) and the source, provide a link to the Creative Commons licence, and indicate if you modified the licensed material. You do not have permission under this licence to share adapted material derived from this article or parts of it. The images or other third party material in this article are included in the article's Creative Commons licence, unless indicated otherwise in a credit line to the material. If material is not included in the article's Creative Commons licence and your intended use is not permitted by statutory regulation or exceeds the permitted use, you will need to obtain permission directly from the copyright holder. To view a copy of this licence, visit <http://creativecommons.org/licenses/by-nc-nd/4.0/>.

Conclusions These findings provide additional insights into the link between breast cancer and PMG, offering potential strategies for breast cancer management and treatment.

Keywords Pyrimidine metabolism, Gene signature, Breast cancer, POLR2C

Introduction

Breast cancer is one of the most common malignant tumors among women worldwide and remains a major disease threatening women's life and health [1]. Although significant progress has been made in breast cancer treatments, including surgery and drug therapy, recurrence, progression and increased mortality due to drug resistance and metastasis continue to be major challenges in clinical treatment [2–4]. Therefore, exploring novel biomarkers and developing new therapeutic targets are crucial for improving clinical outcomes and advancing breast cancer research.

Metabolic reprogramming is considered a key hallmark of cancer. Malignant cells reprogram metabolic pathways to cope with a variety of intrinsic and extrinsic defects in cell survival and growth [5]. In this process, the metabolism of sugars, lipids, and amino acids ultimately affects tumor growth through nucleotide metabolism. Among the complex nucleotide metabolic pathways, pyrimidine biosynthesis is conserved across all organisms and is essential for maintaining basic cellular functions, including DNA and RNA biosynthesis [5].

A substantial body of evidence indicates that dysfunction in pyrimidine metabolism (PM) is closely related to the progression of breast cancer. Drugs targeting pyrimidine metabolism have already been approved for the treatment of breast cancer [6, 7]. Furthermore, with the advancement in sequencing technology, models based on differences in pyrimidine metabolism-related genes have been established for various tumors, such as gastric cancer, colorectal cancer, and bladder cancer [8, 9]. Therefore, identifying differentially expressed genes in pyrimidine metabolism holds significant promise for the treatment and prognosis of breast cancer. In this study, we constructed a pyrimidine metabolism (PM) risk model based on genes related to this pathway to assess the metabolic risk status of breast cancer patients. Additionally, the hub gene POLR2C was further identified and verified as a potential prognostic marker. Targeting POLR2C in combination with anti-PD-1 and anti-angiogenic therapies demonstrated suggested a potential therapeutic direction.

In conclusion, our study underscores the critical role of PM in breast cancer progression and highlights the potential of PM as a predictive tool for patient prognosis. Our findings indicate that PM is closely related with immunology, providing evidence that combined immunotherapy with metabolic medicine might be a feasible treatment. Furthermore, POLR2C, identified as a hub

gene in our study, demonstrated a significant relationship with estrogen, warranting further investigation. These findings expand our understanding of the interactions between PM and breast cancer, particularly in the context of tumor proliferation and treatment strategies.

Methods

Data acquisition

The transcriptome data and clinical data were obtained from the TCGA-BRCA cohort (<https://www.cancer.gov/tcga>). The TPM value of transcriptome data were utilized in the clustering of BRCA patients.

The protein level of POLR2B and POLR2C were accessed in the ULCAN database (UALCAN (uab.edu)) [10] of the Clinical Proteomic Tumor Analysis Consortium (CPTAC) project. And the immunohistochemistry results were obtained in the Human Protein Atlas.

Consensus clustering

The subtypes of BRCA samples were evaluated by the R package ConsensusClusterPlus [11]. The datasets were clustered by the Euclidean squared distance metric and the K-means algorithm with k from 2 to 9. The optimal k value was determined by the cumulative distribution function (CDF) curve.

Calculation of the risk score

The univariable Cox regression analysis was firstly used to filter clinical-related variables. Then the LASSO regression was performed using the R package glmnet to establish a mathematical prediction model calculating the PM risk scores (RS) of the patients. 10-fold cross-validation (cv.glmnet) were used to determine the optimal lambda value (lambda.min) and select the most predictive genes, which helps reduce overfitting and improve the generalizability of the model. The RS of each patient was calculated by the mathematical formula:

$$\begin{aligned} PM \text{ risk score} &= 0.004844 \times CDA + 0.002563 \times DUT + 0.000139 \times NME6 \\ &+ 0.315789 \times NT5C1A + 0.008599 \times NT5E + 0.02936 \\ &\times POLR2B + 0.004527 + 0.00503 \times POLR2K \\ &- 0.012861 \times POLR3GL + 0.02145 \times UPRT \end{aligned}$$

Survival analysis

To obtain the best cutoff point to classify samples into high and low expression groups, the surv_cutpoint command was used according to the TPM value of a specific gene. Then, a log-rank test was applied to examine the

outcome results by the Kaplan–Meier method. R packages KMsurv, survival, and survminer were used to conduct prognostic analysis.

And the external KM analysis results were obtained from the PanCanSurvPlot website.

Evaluation of immune cell infiltration

Two immune infiltration methods including CIBERSORT and MCPCounter were utilized to evaluate the immune cells infiltration in each sample.

Biological pathway enrichment analysis

The Gene Ontology (GO) and the hallmark gene set enrichment analysis were conducted using the R package clusterProfiler and gene sets downloaded from the R package org.Hs.eg.db and the Molecular Signatures Database (MSigDB) with the aid of R package msigdb. Pathways with a p -value < 0.05 and false discovery rate (FDR) < 0.05 were considered significant.

Single cell RNA analysis

The single cell RNA analysis, which showed the TPM value of a specific gene in each cell type and the gene-related pathways, was conducted in the TISCH2 [12] and CancerSEA [13] website respectively.

Cell culture

Human and mouse TNBC cell lines (MDA-MB-231, BT-549 and 4T1) were purchased from the Cell Bank/Stem Cell Bank, Chinese Academy of Sciences (Shanghai, China). Briefly, the cells were cultured in high-glucose DMEM (Thermo Fisher Scientific, CA, USA) supplemented with 10% fetal bovine serum (Gibco, Life Technologies) in an incubator at 37 °C and 5% CO₂.

Wound healing assay

Cells were seeded onto 6-well culture plates at 4×10^5 cells/well. A sterile micropipette tip was used to scratch the confluent monolayers in straight lines. After the cells were treated, they were allowed to recover from the wounds for 48 h. Pictures of the same wound position were recorded at the time of scratching and after 48 h under a microscope. The migration results were evaluated using ImageJ software.

Cell migration and invasion assays

Cell migration and invasion were assessed as previously described [14]. Transwell chamber assays were designed with 8 μm pores and 6.5 mm polycarbonate transwell filters. In brief, cells were seeded in the upper chamber at a concentration of 2.5×10^5 cells/ml in a medium without serum. Medium containing 10% FBS was subsequently added to the bottom chamber. The cells were fixed with 4% paraformaldehyde for 20 min and stained with crystal

violet for 30 min after cell migration or invasion for 36 h. The cells on the surface, without migration or invasion, were removed by scraping. Finally, a microscope was used to count the number of invaded cells.

Western blot

Western blot analysis was conducted as described in our previous study [15]. Whole-cell lysates were extracted using radioimmunoprecipitation assay (RIPA) lysis buffer supplemented with a protease inhibitor cocktail (Sigma, USA). The proteins were separated by sodium dodecyl sulfate-polyacrylamide gel electrophoresis (SDS-PAGE) and then transferred onto polyvinylidene difluoride (PVDF) membranes (Millipore, Bedford, USA). The membranes were incubated with primary antibodies (Supplementary Table S1) at 4 °C overnight. The membranes were then probed with an HRP-conjugated secondary antibody (Beyotime, Shanghai, China) at 25 °C for 1 h, followed by washing with Tris Buffered Saline and 0.05% Tween 20 (TBST) three times for 10 min each. Finally, the membranes were visualized and imaged with an enhanced chemiluminescence system.

IHC

Paraffin-embedded mouse tumor tissue samples were cut into 4–5 μm thick sections and subjected to immunohistochemical studies. IHC staining was performed on mouse tumor samples or tissue microarrays following a standard protocol by incubation with primary antibodies overnight, followed by incubation with horseradish peroxidase (HRP)-conjugated secondary antibodies for 1 h at room temperature. The proteins were detected by IHC and analyzed by two independent pathologists. Immunoreactivity was scored under the H-score system by two investigators according to the percentage of positively stained cells (graded on a scale of 0–4: 0, $< 5\%$; 1, 5–25%; 2, 25–50%; 3, 50–75%; and 4, $> 75\%$) and the intensity of staining (graded on a scale of 0–3: 0, negative; 1, weak; 2, moderate; and 3, strong), with total scores ranging from 0 to 12³⁰. Based on the immunoreactivity scores, the proteins detected were categorized into low expression (H score < 4) or high expression (H score ≥ 4) groups.

In vivo assays

Five- to six-week-old female BALB/c mice, weighing approximately 20–25 g, were purchased from the Shanghai Laboratory Animal Company. All animal experiments were approved by the Animal Ethics Committee of Ruijin Hospital and performed according to the “Guide for the Care and Use of Laboratory Animals” by the National Academy of Sciences (Washington, DC, USA). The detailed procedures of the animal experiments used in this study are described in Supplementary Figs. 3 and 4. The orthotopic tumor tissues were harvested for RNA

sequencing, immunohistochemistry, or immunofluorescence after the mice were sacrificed. The lung tissues from the metastatic model were harvested for hematoxylin and eosin-stained after the mice were sacrificed.

Immunofluorescence (IF) staining

Sterilized coverslips were placed on the bottom of a 6-well plate. The cells were subsequently seeded on coverslips at a density of 1×10^6 in each well. After the cells were treated, the coverslips were fixed with 4% paraformaldehyde for 15 min, followed by permeabilization of the cells in 0.2% Triton X-100 for another 20 min. The cells were then stained with primary antibodies for a 12-hour incubation at 4 °C. The cells were subsequently incubated with a secondary antibody for 1 h at 4 °C in the dark. Finally, DAPI was used to label the nuclei. The cells were photographed and recorded using a fluorescence microscope (Lexcel Lasers, Fremont, CA) [16].

Statistical analysis

All analyses were performed using R 4.1.3. All statistical tests were two-sided, and a P -value < 0.05 was considered statistically significant unless otherwise noted. Continuous variables that conformed to normal distribution were compared using an independent t-test for comparison between groups, whereas continuous variables with skewed distribution were compared with the Mann-Whitney U-test.

Results

Identification of pyrimidine metabolism clusters

A total of 108 pyrimidine metabolism-related genes were identified from the MSigDB KEGG pathways. We utilized the consensus clustering method to differentiate the expression patterns among breast cancer patients. As illustrated in Fig. 1A, the optimal number of clusters was determined to be $k=3$. Figure 1B shows that the clustering results were satisfactory. Based on the clustering results, we discovered significant survival differences among three PM clusters. Specifically, PM cluster C exhibited the worst overall survival probability. In terms of clinical classification, PM cluster C had smallest proportion of stage I patients and the highest percentage of stage II patients. Additionally, patients in PM cluster C were more likely to have advanced T stages. However, there were no significant differences in M stages and N stages among clusters (Fig. 1D). Figure 1E summarizes the overall expression patterns of PM gene signatures among three clusters, where clear variances were observed.

Biological pathway differed among PM clusters

To understand why PM cluster C had worst survival status among clusters, we performed KEGG enrichment

analysis and GSEA analysis of the HALLMARK gene sets. Compared to PM cluster A, differentially expressed genes (DEGs) in cluster C were enriched in numerous pathways related to cell proliferation including the KEGG cell cycle, KEGG DNA replication and KEGG pyrimidine metabolism pathways, indicating the PM cluster A had comparatively low pyrimidine metabolic activity (Fig. 1F). When compared to PM cluster B, PM cluster C had more DEGs associated with tumor cells proliferation, such as the KEGG WNT signaling pathway and KEGG cell cycle. Cluster C was also correlated with various cancer-related pathways, including the KEGG small cell lung cancer, KEGG glioma and the KEGG renal cell carcinoma (Fig. 1G).

Comparatively, PM cluster A exhibited enrichment of the KEGG JAK STAT signaling pathway and the KEGG TGF-beta signaling pathway, with inactivity in the KEGG pyrimidine metabolism pathway, indicating the distinct metabolic modes in cluster A (Fig. 1H). The Venn diagram illustrated significant DEGs among the three clusters (Fig. 1I). Further analysis of the DEGs in cluster C compared to the other two PM clusters showed that cluster C had more pathways related to proliferation, including the HALLMARK E2F targets, HALLMARK G2M checkpoint and the HALLMARK mitotic spindle. Additionally, cluster C was enriched in pathways related to cancer progression, such as HALLMARK MYC targets V1 and the HALLMARK MTORC1 signaling (Fig. 1J). In summary, the excessive and uncontrolled activation of cancer-related pathways in PM cluster C may contribute to the most unfavorable survival outcomes observed in patients within this cluster.

Establishment of the PM risk model

To better evaluate the prognostic impact of PM genes, we first performed univariate Cox analysis to identify the genes most related to patient survival, resulting in the selection of 12 PM genes (Fig. 2A). Based on the LASSO analysis, 10 out of 12 PM genes were ultimately determined for the establishment of the PM risk model (Fig. 2B). Figure 2C shows the distribution of PM risk score among breast cancer patients and the cut-off value for defining high- and low-risk subgroups. Figure 2D illustrates the survival status and survival time of each subgroup. Compared to the low-risk subgroup, the high-risk subgroup exhibited elevated expression of PM genes, except for POLR3GL (Fig. 2E).

The KM plot confirmed that high-risk subgroup had significantly worse overall survival (Fig. 2F). The ROC curve indicated that the prognostic value of the PM risk score was robust (Fig. 2G). Based on univariable and multivariable Cox analysis, the risk score was found to be an independent indicator of patient survival with stable prognostic value (Fig. 2H and I). Furthermore, a

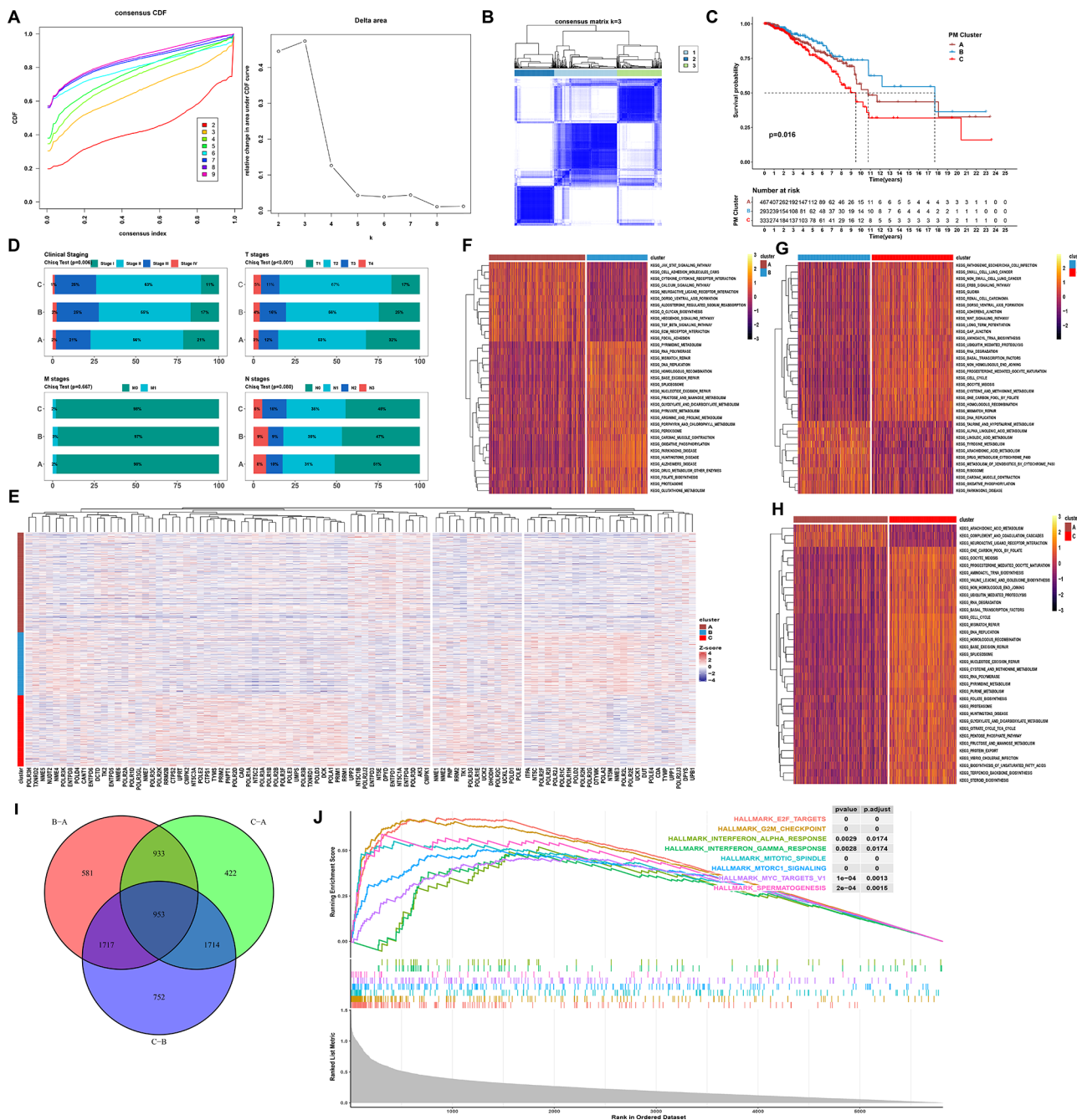


Fig. 1 Consensus clustering of breast cancer using pyrimidine metabolism related genes. **(A)** The consensus cumulative distribution function (BCD) and **(A)** delta area plot revealed that k=3 was best for clustering. **(B)** Consensus matrix for k=3. **(C)** KM plot displayed the survival differences among three pyrimidine metabolism (PM) clusters. **(D)** Bar plot showed the proportion of samples with distinct clinical stages, T stages, M stages and N stages. **(E)** Heatmap showed the different expression patterns of modeled genes in three PM clusters. Differences in biological pathways among three PM clusters. **(F-H)** Differences in KEGG pathways between each PM cluster. **(I)** Venn diagram showing the overlap among datasets **A**, **B**, and **C**. **(J)** Differences in Hallmark pathways between each PM cluster

nomogram was constructed to evaluate 1-, 3- and 5-year survival based on clinical staging and risk score (Fig. 2J). The nomogram demonstrated good performance in predicting both 3- and 5-year survival as validated by the calibration results (Fig. 2K).

The differences in immune landscape between two risk subgroups

As illustrated in Fig. 3A, the Stromal Score, Immune Score and ESTIMATE Score were significantly higher in the low-risk subgroup. Using the IPS method, we found that the high-risk subgroup had a higher presence of

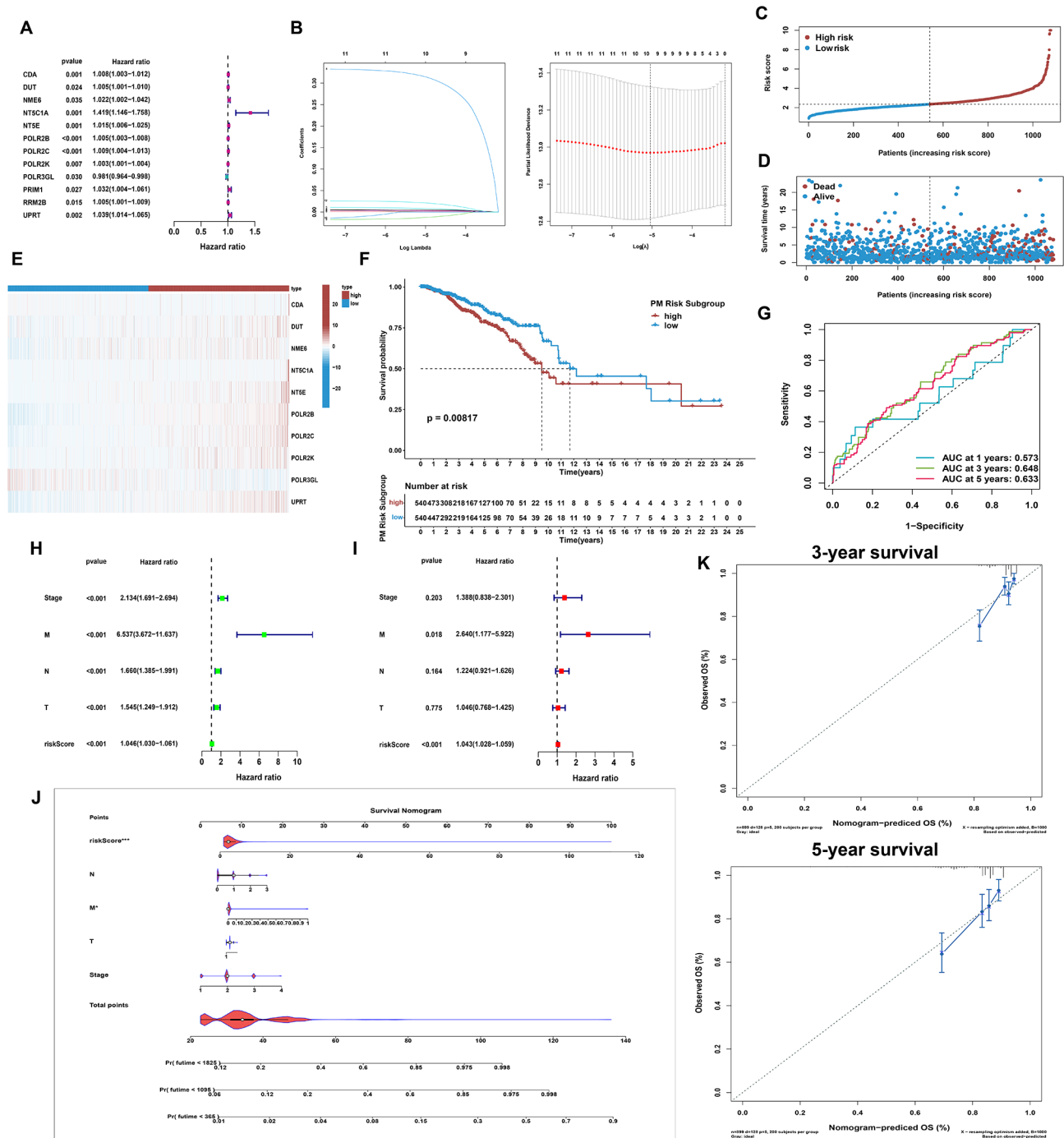


Fig. 2 Establishment of the PM risk model. **(A)** Univariable Cox results of the PM genes in breast cancer. **(B)** LASSO results determined 10 PM genes for the establishment of PM risk model. **(C)** Determination of the high and low risk subgroups. **(D)** Patient survival status with increasing risk score. **(E)** Expression patterns of 10 modeled genes in high and low risk subgroups. **(F)** ROC plot displayed the efficacy of risk model. Establishment of the nomogram. **(H)** Univariable Cox and **(I)** multivariable Cox results revealed PM riskScore was robust in predicting patient survival. **(J)** Establishment of the nomogram. **(K)** Calibration results of the nomogram in predicting 3- and 5- year survival of breast cancer patients

MHC molecules and effector cells (EC), but fewer suppresser cells (SC). Moreover, using CIBERSORT and MCPCounter, we evaluated the estimated proportion and infiltration of specific immune cell types. The

infiltration of T cells, particularly CD8⁺ T cells, was greater in the low-risk subgroup. In contrast, the high-risk subgroup had higher estimated proportions of M2 macrophages and neutrophils, which are correlated with

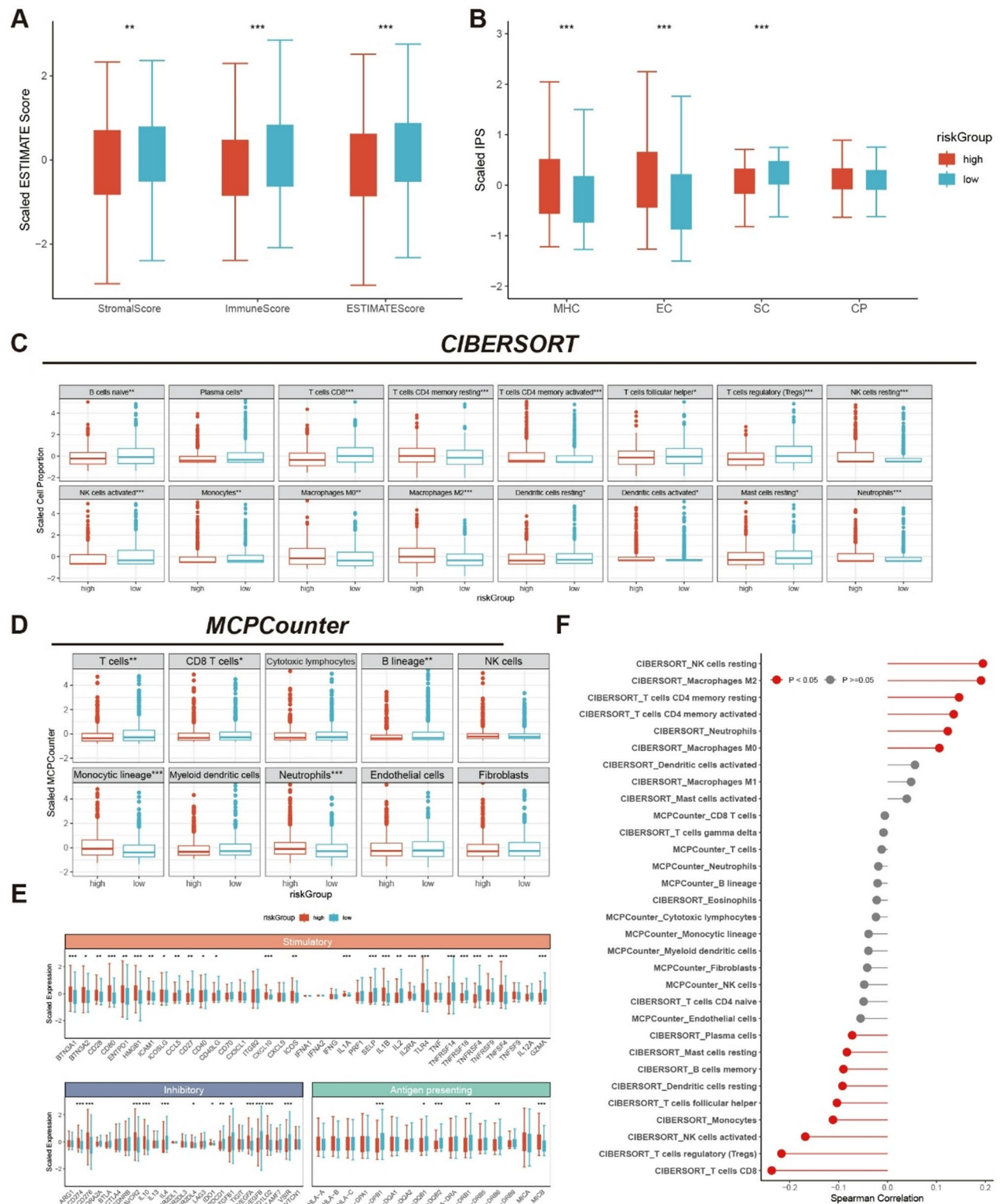


Fig. 3 Correlation of risk score with the immune landscape of breast cancer. Boxplot showed the (A) ESTIMATE score and (B) IPS score in two risk subgroups. (C-D) Boxplot displayed the significant CIBERSORT results of estimated cell proportion and all MCPCounter results among two subgroups. (E) Boxplot showed the different expression patterns of stimulatory, inhibitory and antigen presenting gene signatures among two risk subgroups. (F) Spearman correlation score of risk score with CIBERSORT and MCPCounter score

worse survival in breast cancer (Fig. 3C and D). The stimulatory immune checkpoints showed distinct preferences in the two risk subgroups. Regarding inhibitory immune checkpoints, canonical immune checkpoints like CD274, IDO1, PDCD1LG2 were more abundant in the high-risk subgroup. Antigen-presenting molecules, including HLA-DPB1, HLA-DQB1, HLA-DQB2, HLA-DRB1 and HLA-DRB6, had significantly higher expression level in the low-risk subgroup. To quantify the correlation strength between risk score and the estimated immune cells, the Spearman correlation analysis indicated the risk score was significantly positively associated with M2 macrophages and neutrophils, as estimated by the CIBERSORT method and negatively correlated with the CD8⁺ T cells (Fig. 3F).

Recognition of the hub PM gene signatures and their prognostic value

Of all the 10 modeled genes, we filtered those that had the same correlation tendency with risk score, specifically, those significantly correlated with M2 macrophages and negatively with CD8⁺ T cells. We used a Spearman correlation score greater than 0.1 as the minimum threshold (Fig. 4A). Four of the modeled genes met this correlation, and we further explored which cells expressed these genes the most, using single cell RNA sequencing data. As illustrated in Fig. 4B and E, among the various cell types, malignant cells consistently showed high expression of NME6, POLR2B and POLR2C, while UPRT had relatively low expression in all cell types.

Given the relatively low expression of UPRT in breast cancer cells, we focused on the other three PM genes for further research. Using the CancerSEA website, we explored the expression of specific PM genes and their correlation with pathway activity. A significant proportion of breast cancer cells expressed NME6, POLR2B and POLR2C (Fig. 4F and H). While NME6 expression in breast cancer cells showed no consistent correlation with numerous cancer-related pathways (Fig. 4G), the expression of POLR2B and POLR2C was robustly correlated with DNA damage and DNA repair, indicating their role in tumor initiation and progression (Fig. 4F and H).

To validate the prognostic value of POLR2C, we analyzed external datasets with overall survival (OS) or recurrence free survival (RFS) data. The results showed that, across multiple datasets and using medium expression level as criteria for patient division, POLR2C consistently performed well in predicting patient OS (Fig. 5A) and RFS (Fig. 5B). In summary, POLR2C may serve as a key hub PM gene in breast cancer.

Knockdown of POLR2C reduces EMT and angiogenesis and immunosuppression

To further investigate the role of POLR2C in TNBC progression, we first constructed shNC and shPOLR2C TNBC cell lines. Wound healing and transwell assays demonstrated that knocking down POLR2C inhibited tumor migration and invasion (Fig. 6A-D). Next, the orthotopic tumor model was established using 4T1 cells. The shNC group exhibited significant tumor growth, as evidenced by increases in tumor weight and volume (Fig. 6G-I). Additionally, the shNC 4T1 group showed more lung metastases (Fig. 6J).

To determine whether shPOLR2C tumor cells can suppress epithelial-mesenchymal transition (EMT) and angiogenesis in the tumor microenvironment (TME), we performed RNA-seq on tumor tissues from three negative control (NC) mice and three shPOLR2C mice. Differential gene expression analysis and unsupervised clustering revealed two distinct groups (Fig. 7A, Figure S1A, B). As shown in the bar plot and volcano plot, 613 upregulated genes and 609 downregulated genes were identified between the two groups (Figure S1C, D).

GO and KEGG analyses were conducted to study the functions of the differentially expressed genes (DEGs) based on RNA-seq data. GO analysis indicated that the upregulated DEGs were enriched in terms related to immune cell responses in Biological Process (BP) and immune receptor activation in Molecular Function (MF) (Figure S1A). GO chord diagram analysis showed significant enrichment of pathways related to angiogenesis, EMT, and immune regulation. Pathways such as “regulation of angiogenesis” and “positive regulation of myeloid leukocyte immunity” were significantly downregulated, indicating that POLR2C knockdown impaired angiogenesis. This disruption may affect the TME by limiting oxygen and nutrient supply. Key genes involved in EMT and cell adhesion, including VCAM1, CX3CR1, and ICAM2, were also downregulated. These findings suggest that cell migration and plasticity were suppressed, which are hallmarks of EMT, potentially reducing metastatic potential (Fig. 7B).

KEGG pathway enrichment analysis revealed that pathways related to EMT, such as “cell adhesion molecules” and “leukocyte transendothelial migration,” were significantly downregulated in shPOLR2C tumors. This indicates impaired cell adhesion and migration, suggesting that POLR2C knockdown inhibits EMT and reduces tumor cell invasion and metastasis. Immune-related pathways, including “NF-kappa B signaling,” “Toll-like receptor signaling,” and “natural killer cell-mediated cytotoxicity,” were also downregulated. This suggests that immune evasion mechanisms were disrupted, potentially improving immune surveillance and anti-tumor immune responses (Fig. 7C, Figure S1B). Reactome pathway

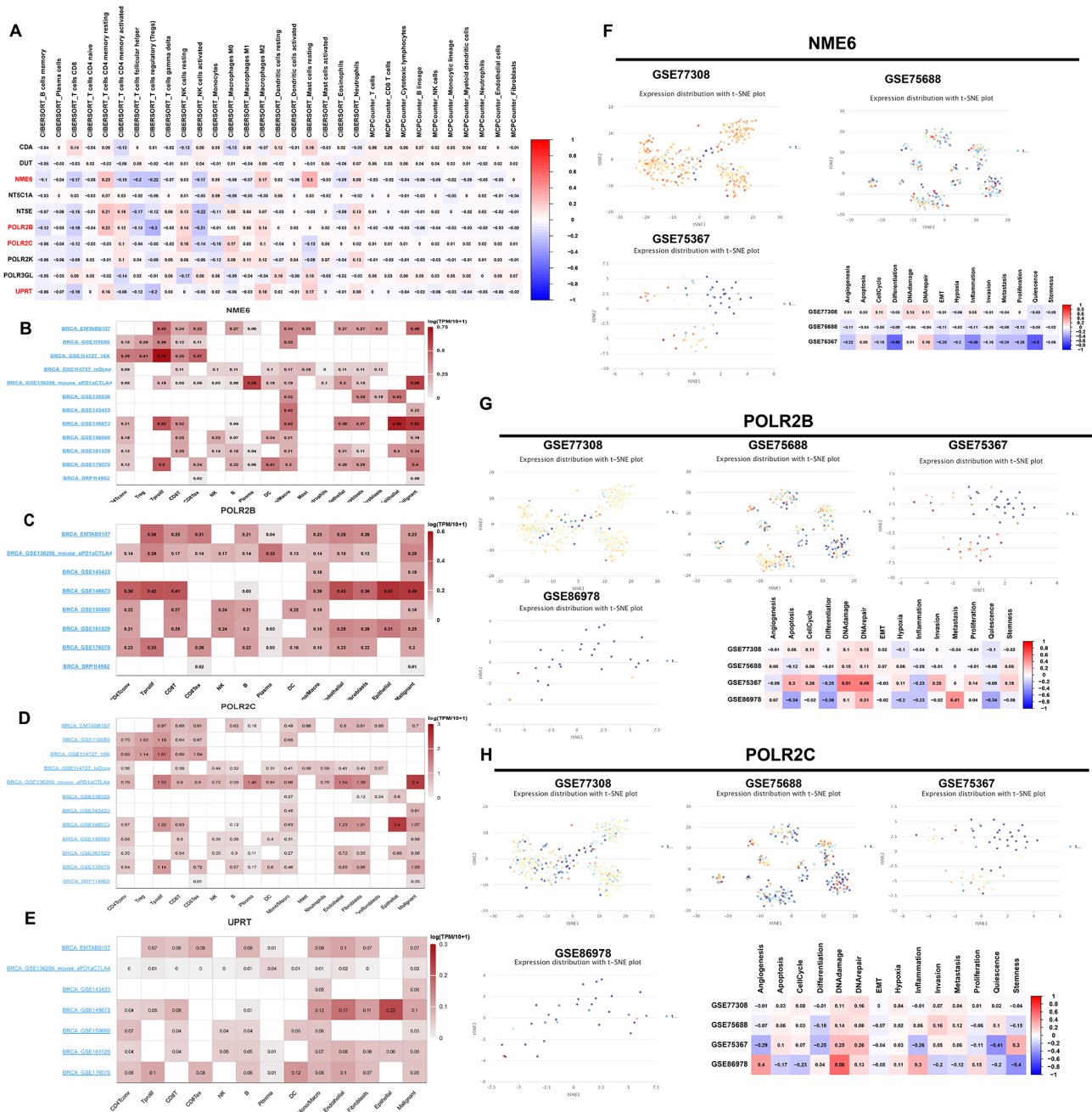


Fig. 4 Determination of the hub PM genes. **(A)** Spearman correlation score of modeled PM genes with CIBERSORT and MCPCounter score. **(B-E)** The expression patterns of hub PM genes in single cell RNA datasets of distinct cell types. Correlation of hub PM gene expression with cancer-related pathway activities. The expression level of NME6, POLR2B and POLR2C in each single cell RNA datasets. **(F-H)** The correlation score between hub PM gene expression and cancer-related pathways

enrichment analysis also supported these conclusions (Supplementary Figure S1C).

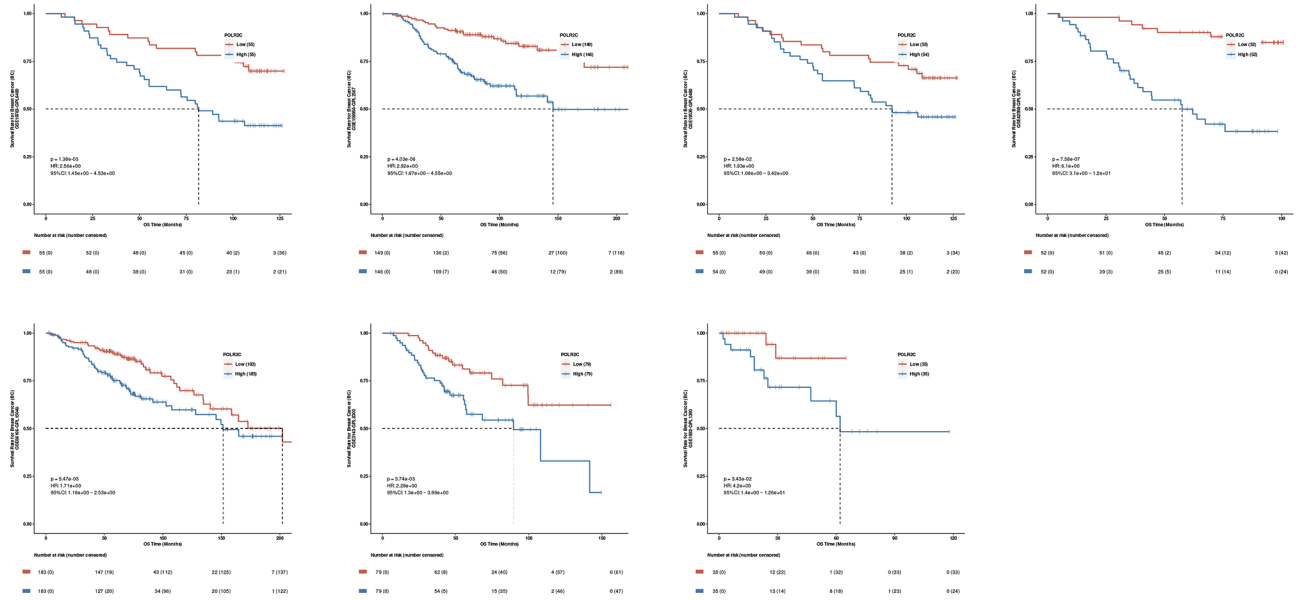
GSEA further analyzed pathways related to angiogenesis and EMT. EMT signature gene sets, VEGF signaling pathways, and angiogenesis regulatory pathways were all enriched in the downregulated region, indicating that downregulated DEGs may lead to reduced expression of EMT-related and angiogenesis-related genes (Fig. 7D, E).

Gene set variation analysis (GSVA) showed that enrichment of angiogenesis and EMT decreased in shPOLR2C tumors compared to NCs (Fig. 7F).

Finally, CIBERSORT analysis was used to compare the relative levels of different immune cell types in NC and shPOLR2C tumors. CD8⁺ T cells and T follicular helper cells were significantly increased in shPOLR2C tumors,

A

OS



B

RFS

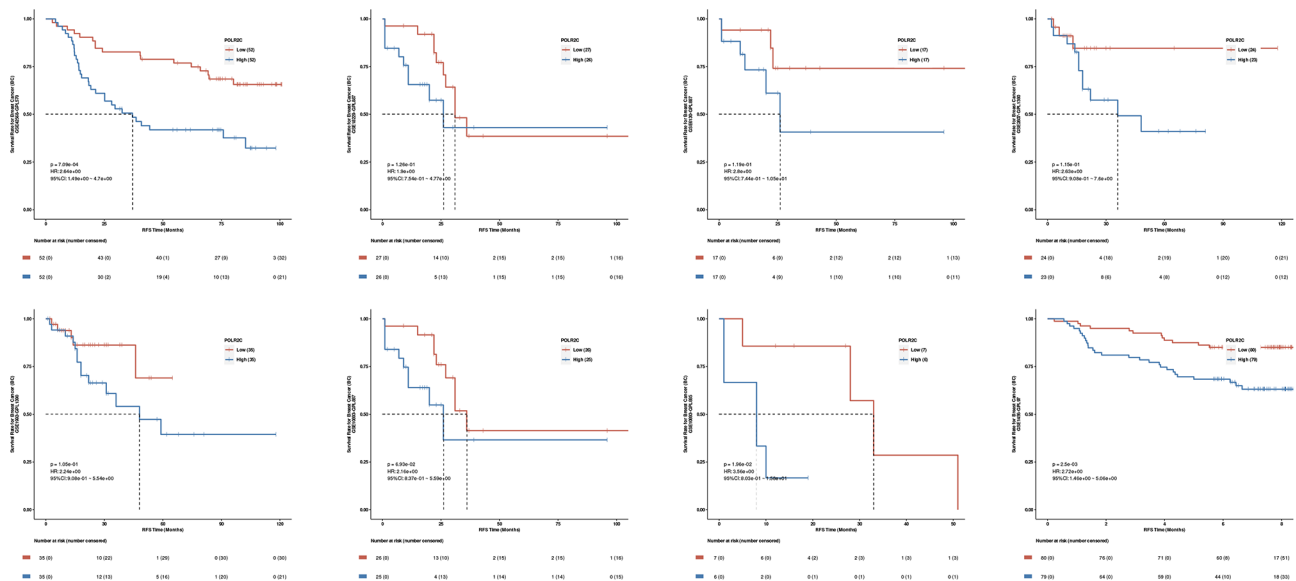


Fig. 5 The protein level of hub PM genes. **(A)** KM plot showed the OS data from GSE19783, GSE159956, GSE19536, GSE42568, GSE86166, GSE3143 and GSE1992 datasets. **(B)** KM plot showed the RFS data from GSE42568, GSE1456, GSE10893, GSE1992, GSE18229, GSE2607 and GSE6130 datasets

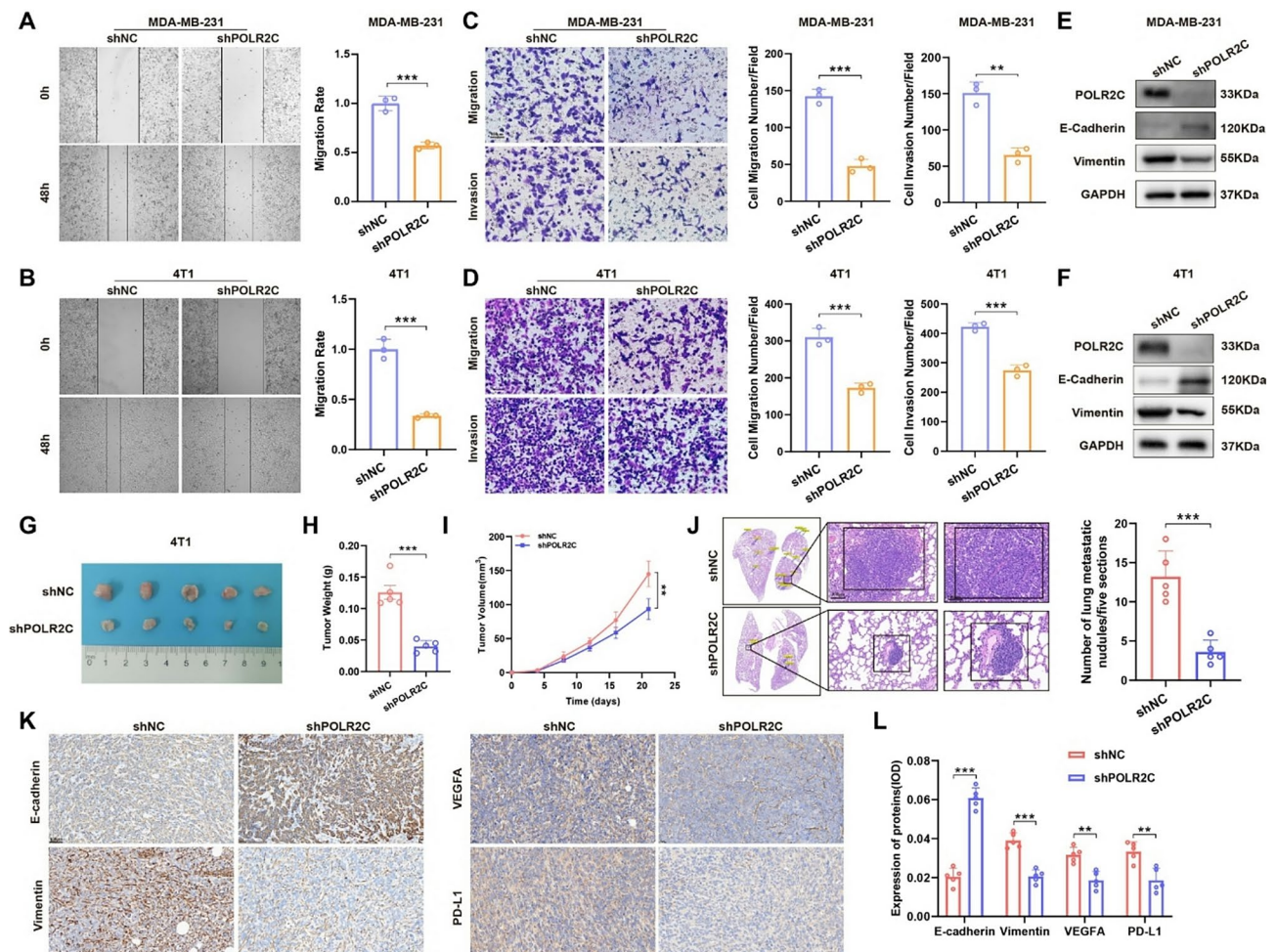


Fig. 6 Knockdown of POLR2C reduces EMT and angiogenesis and immunosuppression. **(A)** Representative images of wound healing assays and statistical analysis in the shNC MDA-MB-231 cell and the shPOLR2C MDA-MB-231 cell. **(B)** Representative images of wound healing assays and statistical analysis in the shNC 4T1 cell and the shPOLR2C 4T1 cell. **(C)** Representative images of transwell assays and statistical analysis in the shNC MDA-MB-231 cell and the shPOLR2C MDA-MB-231 cell. **(D)** Representative images of transwell assays and statistical analysis in the shNC 4T1 cell and the shPOLR2C 4T1 cell. **(E, F)** Validation of POLR2C and markers of EMT between shNC tumor cells and shPOLR2C tumor cells via Western blot. **(G-I)** Images of orthotopic tumors in BALB/c mice in the shNC 4T1 group and the shPOLR2C 4T1 group. Tumor volumes in BALB/c mice are shown at the time of sacrifice. Line graph comparing the tumor growth of BALB/c mice. **(J)** Representative images and statistical calculation of tumor metastatic nodules in HE-stained lung sections from BALB/c mice. **(K, L)** IHC staining and statistical analysis of EMT-related markers, angiogenesis-related markers and immune markers in tumors from BALB/c mice

while M2 macrophages were reduced (Fig. 7G, Figure S1D).

Subsequent *in vivo* and *in vitro* assays confirmed that knockdown of POLR2C inhibited the tumor EMT process and angiogenesis (Fig. 6E-F, K-L, Figure S1).

Collectively, the knockdown of POLR2C impairs angiogenesis and EMT by downregulating key pathways and genes, while enhancing anti-tumor immunity through modulation of immune cell infiltration and activation within the TME.

Targeting POLR2C combined with anti-PD-1 immunotherapy and anti-angiogenesis therapy inhibits TNBC growth and metastasis

Based on the aforementioned studies, we further investigated the efficacy of combining immunotherapy and anti-angiogenic therapy with targeted POLR2C inhibition.

A BALB/c orthotopic tumor model was established using 4T1 cells, and the mice were randomly divided into four groups: control, anti-PD-1 combined with anti-VEGFA, shPOLR2C and shPOLR2C combined with anti-PD-1 and anti-VEGFA. Compared with control group, the use of anti-PD-1 antibody and Bevacizumab was more effective in inhibiting tumor growth and reducing lung metastases (Fig. 8A, B). Additionally, the

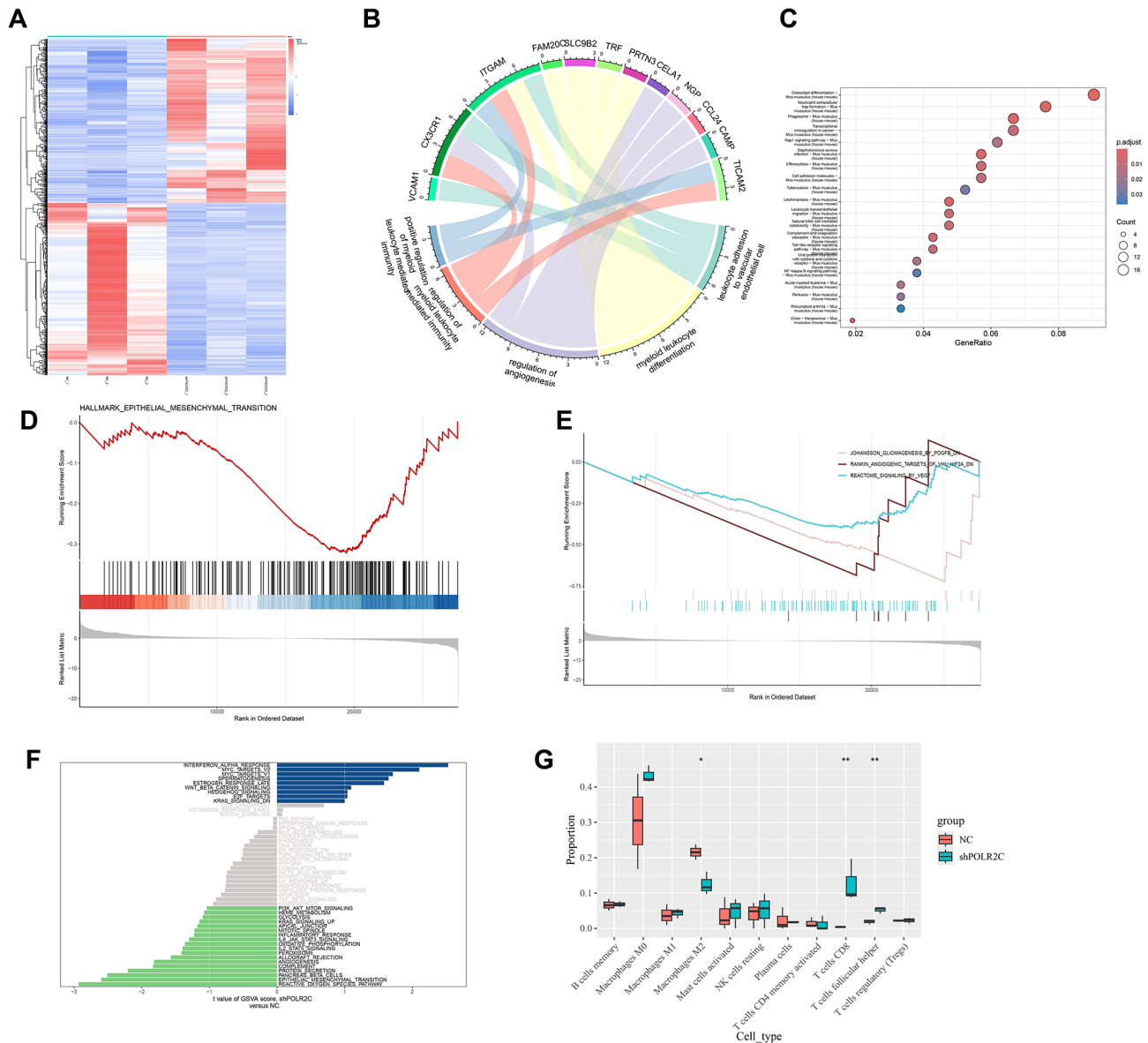


Fig. 7 The analysis of RNA-seq on tumor tissues. **(A)** Heatmap showed the different expression genes in two groups. **(B)** GO chord diagram analysis. **(C)** Dot plot of different KEGG pathways in two groups. **(D)** GSEA enrichment of hallmark of epithelial-mesenchymal transition. **(E)** GSEA enrichment of angiogenesis related pathways. **(F)** GSEA enrichment in Hallmark pathways between two groups. **(G)** Differences in immune cells expressions in CIBERSORT between two groups

combination treatment showed a greater ability to inhibit EMT process of tumor, as evidenced by immunohistochemistry and immunofluorescence analysis (Fig. 8C-H).

Discussion

To gain the energy required for tumor growth and invasion, cancer cells accelerate the exchanges of biomolecules such as sugars, amino acids, lipids and nucleic acids through various metabolic pathways, leading to reprogrammed metabolites [17–19]. Increased glycolysis activates biosynthetic pathways like pyrimidine and purine, whose materials are supplied by glycolytic cycle

[20]. Recent research has shown that pyrimidine synthesis can facilitate chemotherapy resistance in breast cancer cells via adaptive metabolic reprogramming [21]. Based on these theories, we explored the landscape of pyrimidine metabolism in breast cancer using comprehensive bioinformatics and statistical analysis, validated with public datasets.

Using consensus clustering, we grouped 108 PM-related genes into three clusters, with Cluster C identified as the most correlated with aggressive cancer behavior and worst prognosis, indicating the link between specific PM profiles and breast cancer progression. This

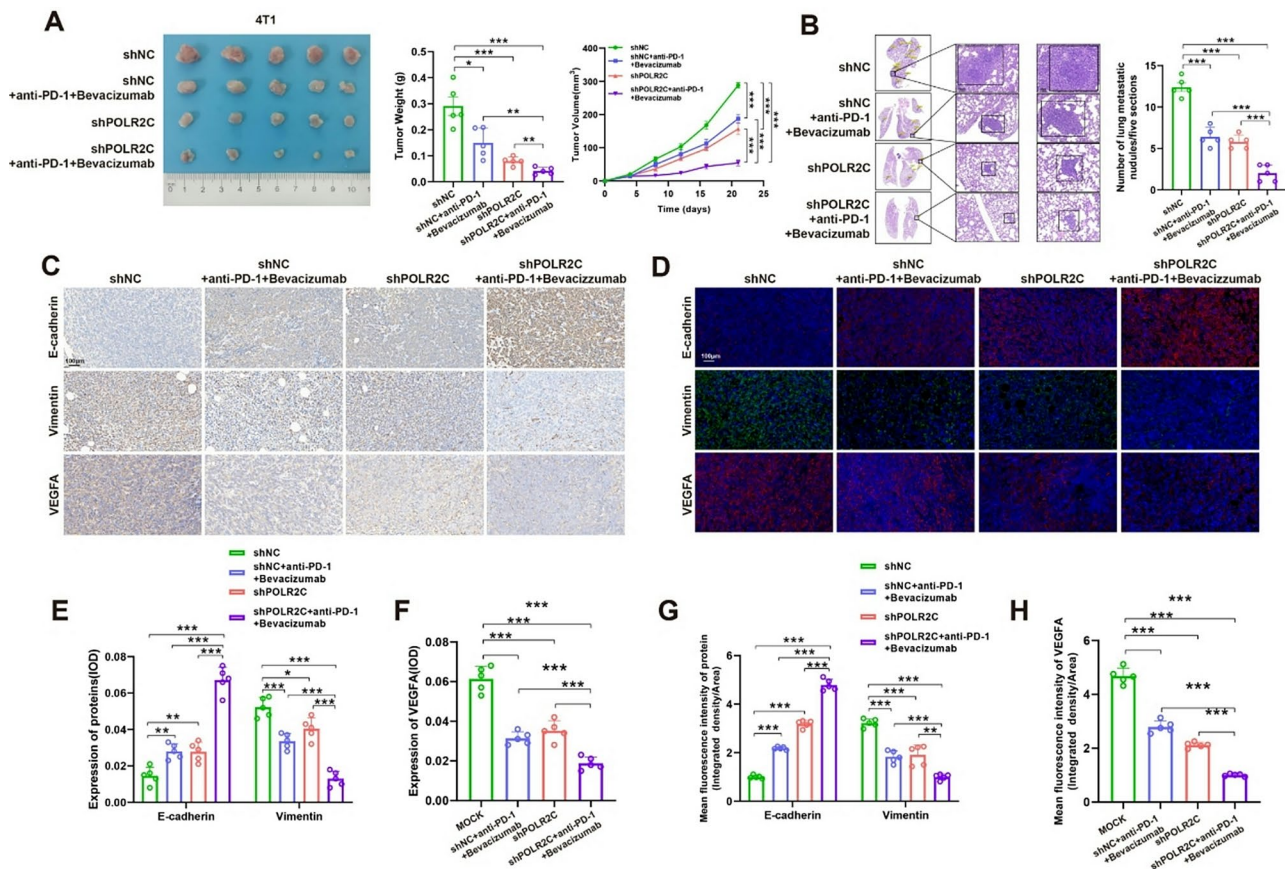


Fig. 8 Targeting POLR2C combined with anti-PD-1 immunotherapy and anti-angiogenesis therapy inhibited TNBC growth and metastasis in preclinical models. **(A)** Photo of excised orthotopic tumors from BALB/c mice in different treatment groups. The injection of the anti-PD-1 antibody (10 μ g once) and Bevacizumab (10 μ g once) or not was scheduled every 3 days. Tumor weights and growth curves of the mice subjected to different treatments are shown. **(B)** Representative images and statistical calculation of tumor metastatic nodules in HE-stained lung sections from metastatic model. **(C-H)** Representative images of IHC and IF staining and statistical analysis of EMT-related markers and angiogenesis-related markers in different treatment groups

finding aligns with the theory that enhanced pyrimidine catabolism and reduced pyrimidine synthesis improve cancer cell death [22]. We analyzed the biological functions and clinical survivals in both individual and pairwise clusters. Our results refined the viewpoint that the metabolic reprogramming of pyrimidine is not limited in proliferation and that the function differ among clusters [23] confirming the validity of our clustering results. To further investigate associations between PM-related gene expressions and breast cancer, we established a PM risk model using Cox and Lasso regression analyses, identifying about 10 genes significantly related to patient survival. This model differentiates patients into high and low-risk groups and has been validated for its prognostic accuracy through Kaplan-Meier survival analysis, ROC curve assessments, and multivariable Cox regression. The PM risk model is the first PM predictive model for breast cancer prognosis, allowing for more personalized management of breast cancer patients based on their metabolic risk profile.

Immunotherapy, including immune checkpoint blockade (ICB) therapies, has been widely applied in breast cancer treatments to reverse cancer immunosuppression and enhance antitumor immunity. Using IPS, CIBERSORT and MCP counter methods, we discovered the correlation of immunity and PM-related genes. Analysis revealed higher immune suppression in the high-risk group, with increased expression of M2 macrophages, neutrophils and immune checkpoints like CD274 and IDO1, and a lower presence of CD8⁺ T cells compared to the low-risk group, which exhibited more robust antigen-presenting features. Recent research on tyrosine kinase inhibitors sequential anti-PD1 immunotherapy in advanced non-small cell lung cancer reported that strategic suppression of CD8⁺ T cell proliferation via inhibition of pyrimidine metabolism enhances the efficacy of ICB by temporally modulating the immune response and reducing metabolic competition between immune cells and tumor cells [24]. Furthermore, M2 macrophages were found to be more abundant in de novo synthesized pyrimidine in both intracellular and extracellular

environments compared to M1 macrophages [25] supporting our data and suggesting that pyrimidine metabolism polarized macrophages alternatively. Additionally, M2 macrophages are highly expressed in Luminal subtypes but not in triple negative ones, indicating a potential link between M2 macrophage activity and hormone receptor-positive tumor microenvironments, which may contribute to chemoresistance in specific subtypes [26]. These findings underscore the potential for combining metabolic therapy with immunotherapy, especially in metabolically high-risk patients. Notably, our PM risk model highlighted an immunosuppressive microenvironment specific to high-risk patients, characterized by the presence of elevated M2 macrophages, neutrophils, and suppressive checkpoints (e.g., CD274/PD-L1). These results suggest that high-risk patients are potentially resistant to PD-1/PD-L1 monotherapy. This is consistent with recent clinical trials that have demonstrated that metabolic reprogramming modulates the efficacy of immunotherapy. For example, in the KEYNOTE-522 trial (NCT03036488), pembrolizumab in combination with chemotherapy improved the rate of pathologic complete remission in TNBC, but a subgroup of patients with immunosuppressive features showed limited benefit [27]. These findings imply that high-risk patients may benefit from combining immune checkpoint blockade with metabolic inhibitors or antiangiogenic agents, but more clinical trials are needed.

Hub PM genes, NME6, POLR2B, and POLR2C, were filtered from the 10 model genes under strict conditions. Among these, POLR2C, an alpha-like 'C' subunit of RNA polymerase II (pol II), showed strong correlations with DNA damage and repair processes, consistent with existing studies [28]. POLR2C mutation which commonly results in low POLR2C expression, are a feature of primary ovarian insufficiency. This is interesting since Luminal subtype breast cancer can be inhibited by endocrine drugs, including aromatase inhibitors and selective estrogen receptor modulators, which work through modulating oestrogen [29]. In addition, POLR2C also shows significant value for cancer itself. In liver cancer, overexpression of POLR2C in animal models can promote the epithelial-mesenchymal transition process through Snail, ultimately promoting liver cancer proliferation and migration [30]. For osteosarcoma, changes in POLR2C expression have been found in clinical samples, and its mRNA expression significantly lower than that of normal osteoblasts [31]. In gastric cancer, analysis of clinical samples showed that POLR2C overexpression is associated with the cisplatin resistance mechanism of gastric cancer [32]. Moreover, immunohistochemistry confirmed higher expression levels of these genes in tumor tissues compared to normal tissues, suggesting their potential as therapeutic targets. The prognostic value of POLR2B

and POLR2C was validated through external datasets with OS and PFS, indicating their potential as prognostic biomarkers. Furthermore, their role in critical cancer pathways suggests they could be pivotal in the development of new treatments focused on metabolic and DNA repair mechanisms. Notably, pyrimidine metabolism is associated with key pathways related to POLR2C function in breast cancer. First, POLR2C is a subunit of RNA polymerase II, and thus its function may not be limited to gene expression changes detected by RNA-seq. This also implies that whether POLR2C affects chromatin accessibility and thus transcription factor binding. ATAC-seq may be able to help explore these questions. In addition, does POLR2C affect RNA modifications? For instance, 5-methylcytosine (m5C) and pseudouridine (Ψ), modifications known to affect mRNA stability and translational efficiency. These issues may be key to note in subsequent POLR2C studies. In addition, our RAN-seq data showed that knocking out POLR2C inhibited angiogenesis-related pathways, as evidenced by the down-regulation of VEGF. In vivo assays demonstrated that anti-POLR2C combined with anti-angiogenic therapy inhibit the metastasis of TNBC. The regulatory mechanism between the POLR2C and VEGF remains to be clarified in future studies.

Comparing with previous studies on PM, we integrated a broader set of PM-related genes into a cluster analysis, identifying distinct groups correlated with clinical outcomes and pathway activities. The establishment of the PM risk model based on this analysis represents an advanced understanding and an application of data, facilitating follow-up researches. Our findings also reveal some critical PM genes that might play significant roles in the process of breast cancer proliferation and metabolic reprogramming.

Our study included the reliance on retrospective data and public datasets, which may not fully capture the dynamic changes in gene expression during the progression of cancer and may introduce selection bias. Due to data availability, our model was primarily trained and validated using TCGA-BRCA, which predominantly represents Western populations. This indeed limits the ethnic and geographic diversity of our findings. Although this study initially revealed the potential value of POLR2C in breast cancer by integrative analysis and functional experiments. However, future studies could be deepened in the following directions. First, the functional characterization and downstream mechanism of POLR2C need to be further explored. These related functional and mechanistic studies need to be validated with more rigorous supportive experiments such as rescue experiments. Additionally, the validation of the pro-tumor functions in POLR2C is not complete, and further experiments are needed both in vivo and in vitro. Second, prospective

studies on the integration of PM features into existing molecular subtyping or multigene detection tools may offer great potential for personalized treatment of breast cancer, which may urgently require follow-up studies. In addition, as mentioned earlier, immunophenotyping studies should also be considered. Finally, the experimental validation of the current manuscript favors the most aggressive TNBC, and more extended studies exploring other molecular subtypes of breast cancer may be needed in the future to extend its applicability.

We plan to explore PM genes, especially POLR2C, using other omics approaches to gain deeper insights into the metabolic reprogramming that occurs in breast cancer cells. Additionally, to extend the PM risk model established in this study, we aim to integrate machine learning techniques or Mendelian randomization to refine the accuracy of prognosis predictions based on comprehensive metabolic, genetic, and clinical data.

In conclusion, our study underscores the critical role of PM in breast cancer progression and highlights the potential of PM as a predictive tool for patient prognosis. PM is closely related with immunology, providing evidence that combining immunotherapy with metabolic therapy might be a feasible treatment. POLR2C, one of the hub PM gene identified in this study, showed its relation to estrogen, warranting further research. These findings will expand the understanding of interactions between PM and breast cancer in its processes of proliferation and treatments.

Supplementary Information

The online version contains supplementary material available at <https://doi.org/10.1186/s12967-025-06700-2>.

Supplementary Material 1

Acknowledgements

Not applicable.

Author contributions

ZW, RW, RH and HW were the core members who conceived and designed the whole article. HW, ZZ, and HZ analyzed the raw data. HW, ZZ, and HZ completed the design and operation of the animal and cell experiments. HW, ZZ, and HZ wrote manuscript draft in the beginning. ZW, KS, and SW revised the final version of the manuscript. All authors have contributed to the study and approved the final version of the manuscript before the process of submitting.

Funding

This work was supported by the National Natural Science Foundation of China (82002773, 82403376, and 82072897).

Data availability

The authors confirm that the data supporting the findings of this study are available within the article and its supplementary materials and further inquiries can be directed to the corresponding authors.

Declarations

Ethics approval and consent to participate

The animal studies were approved by the Medical Ethics Committee of Ruijin Hospital, Shanghai Jiao Tong University. The studies were conducted in accordance with the local legislation and institutional requirements. Written informed consent was obtained from the owners for the participation of their animals in this study.

Consent for publication

Not applicable.

Competing interests

The authors declared that there are no competing interests.

Author details

¹Department of General Surgery, Comprehensive Breast Health Center, Ruijin Hospital, Shanghai Jiao Tong University School of Medicine, Shanghai 200025, China

²Department of Breast Surgery, Fujian Provincial Hospital, Shengli Clinical Medical College of Fujian Medical University, Fuzhou University Affiliated Provincial Hospital, Fuzhou 350001, China

³School of Biomedical Sciences, Li Ka Shing Faculty of Medicine, University of Hong Kong, Hong Kong 999077, China

Received: 12 February 2025 / Accepted: 1 June 2025

Published online: 23 June 2025

References

1. Sung H, Ferlay J, Siegel RL, Laversanne M, Soerjomataram I, Jemal A, Bray F. Global Cancer statistics 2020: GLOBOCAN estimates of incidence and mortality worldwide for 36 cancers in 185 countries. *CA Cancer J Clin.* 2021;71(3):209–49. <https://doi.org/10.3322/caac.21660>.
2. Masuda N, Lee S-J, Ohtani S, Im Y-H, Lee E-S, Yokota I, Kuroi K, Im S-A, Park B-W, Kim S-B, Yanagita Y, Ohno S, Takao S, Aogi K, Iwata H, Jeong J, Kim A, Park K-H, Sasano H, Ohashi Y, Toi M. Adjuvant capecitabine for breast Cancer after preoperative chemotherapy. *N Engl J Med.* 2017;376(22):2147–59. <https://doi.org/10.1056/NEJMoa1612645>.
3. Riggio AI, Varley KE, Welm AL. The lingering mysteries of metastatic recurrence in breast Cancer. *Br J Cancer.* 2021;124(1):13–26. <https://doi.org/10.1038/s41416-020-01161-4>.
4. Wang H, Wang R, Luo L, Hong J, Chen X, Shen K, Wang Y, Huang R, Wang Z. An Exosome-Based specific transcriptomic signature for profiling regulation patterns and modifying tumor immune microenvironment infiltration in Triple-Negative breast Cancer. *Front Immunol.* 2023;14:1295558. <https://doi.org/10.3389/fimmu.2023.1295558>.
5. Wang W, Cui J, Ma H, Lu W, Huang J. Targeting pyrimidine metabolism in the era of precision cancer medicine. *Front Oncol.* 2021;11:684961. <https://doi.org/10.3389/fonc.2021.684961>.
6. Lei P, Wang W, Sheldon M, Sun Y, Yao F, Ma L. Role of glucose metabolic reprogramming in breast Cancer progression and drug resistance. *Cancers (Basel).* 2023;15(13):3390. <https://doi.org/10.3390/cancers15133390>.
7. Chiacchio MA, Iannazzo D, Romeo R, Giorè SV, Legnani L. Pyridine and pyrimidine derivatives as privileged scaffolds in biologically active agents. *Curr Med Chem.* 2019;26(40):7166–95. <https://doi.org/10.2174/092986732566180904125400>.
8. Wu Z, Tan J, Zhuang Y, Zhong M, Xiong Y, Ma J, Yang Y, Gao Z, Zhao J, Ye Z, Zhou H, Zhu Y, Lu H, Hong X. Identification of crucial genes of pyrimidine metabolism as biomarkers for gastric Cancer prognosis. *Cancer Cell Int.* 2021;21(1):668. <https://doi.org/10.1186/s12935-021-02385-x>.
9. Wu Z, Li X, Gu Z, Xia X, Yang J. Pyrimidine metabolism regulator-mediated molecular subtypes display tumor microenvironmental hallmarks and assist precision treatment in bladder Cancer. *Front Oncol.* 2023;13:1102518. <https://doi.org/10.3389/fonc.2023.1102518>.
10. Chandrashekar DS, Karthikeyan SK, Korla PK, Patel H, Shovon AR, Athar M, Netto GJ, Qin ZS, Kumar S, Manne U, Creighton CJ, Varambally S. UALCAN: an update to the integrated Cancer data analysis platform. *Neoplasia.* 2022;25:18–27. <https://doi.org/10.1016/j.neo.2022.01.001>.

11. Wilkerson MD, Hayes DN, ConsensusClusterPlus: A class discovery tool with confidence assessments and item tracking. *Bioinformatics*. 2010;26(12):1572–3. <https://doi.org/10.1093/bioinformatics/btq170>.
12. Han Y, Wang Y, Dong X, Sun D, Liu Z, Yue J, Wang H, Li T, Wang C. TISCH2: expanded datasets and new tools for single-cell transcriptome analyses of the tumor microenvironment. *Nucleic Acids Res*. 2023;51(D1):D1425–31. <http://doi.org/10.1093/nar/gkac959>.
13. Yuan H, Yan M, Zhang G, Liu W, Deng C, Liao G, Xu L, Luo T, Yan H, Long Z, Shi A, Zhao T, Xiao Y, Li X. CancerSEA: A Cancer Single-Cell state atlas. *Nucleic Acids Res*. 2019;47(D1):D900–8. <https://doi.org/10.1093/nar/gky939>.
14. Huang R, Yang Z, Liu Q, Liu B, Ding X, Wang Z. CircRNA DDX21 acts as a prognostic factor and sponge of miR-1264/QKI Axis to weaken the progression of Triple-Negative breast Cancer. *Clin Transl Med*. 2022;12(5):e768. <https://doi.org/10.1002/ctm2.768>.
15. Huang R, Wang H, Hong J, Wu J, Huang O, He J, Chen W, Li Y, Chen X, Shen K, Wang Z. Targeting glutamine metabolic reprogramming of SLC7A5 enhances the efficacy of Anti-PD-1 in Triple-Negative breast Cancer. *Front Immunol*. 2023;14:1251643. <https://doi.org/10.3389/fimmu.2023.1251643>.
16. Huang R, Wang Z, Hong J, Wu J, Huang O, He J, Chen W, Li Y, Chen X, Shen K. Targeting Cancer-Associated Adipocyte-Derived CXCL8 inhibits Triple-Negative breast Cancer progression and enhances the efficacy of Anti-PD-1 immunotherapy. *Cell Death Dis*. 2023;14(10):703. <https://doi.org/10.1038/s41419-023-06230-z>.
17. Xu X, Peng Q, Jiang X, Tan S, Yang Y, Yang W, Han Y, Chen Y, Oyang L, Lin J, Xia L, Peng M, Wu N, Tang Y, Li J, Liao Q, Zhou Y. Metabolic reprogramming and epigenetic modifications in cancer: from the impacts and mechanisms to the treatment potential. *Exp Mol Med*. 2023;55(7):1357–70. <https://doi.org/10.1038/s12276-023-01020-1>.
18. Islam RA, Hossain S, Chowdhury EH. Potential therapeutic targets in energy metabolism pathways of breast Cancer. *Curr Cancer Drug Targets*. 2017;17(8):707–21. <https://doi.org/10.2174/1568009617666170330150458>.
19. Yang K, Wang X, Song C, He Z, Wang R, Xu Y, Jiang G, Wan Y, Mei J, Mao W. The role of lipid metabolic reprogramming in tumor microenvironment. *Theranostics*. 2023;13(6):1774–808. <https://doi.org/10.7150/thno.82920>.
20. Hanahan D, Weinberg RA. Hallmarks of cancer: the next generation. *Cell*. 2011;144(5):646–74. <https://doi.org/10.1016/j.cell.2011.02.013>.
21. Brown KK, Spinelli JB, Asara JM, Toker A. Adaptive reprogramming of de Novo pyrimidine synthesis is a metabolic vulnerability in Triple-Negative breast Cancer. *Cancer Discov*. 2017;7(4):391–9. <https://doi.org/10.1158/2159-8290.CD-16-0611>.
22. Hartleben G, Schorpp K, Kwon Y, Betz B, Tsokanos F-F, Dantes Z, Schäfer A, Rothenaigner I, Monroy Kuhn JM, Morigny P, Mehr L, Lin S, Seitz S, Tokarz J, Artati A, Adamsky J, Plettenburg O, Lutter D, Irmeler M, Beckers J, Reichert M, Hadian K, Zeigerer A, Herzig S, Berriel diaz, M. Combination therapies induce Cancer cell death through the integrated stress response and disturbed pyrimidine metabolism. *EMBO Mol Med*. 2021;13(4):e12461. <https://doi.org/10.15252/emmm.202012461>.
23. Siddiqui A, Ceppi PA, Non-Proliferative. Role of pyrimidine metabolism in Cancer. *Mol Metab*. 2020;35:100962. <https://doi.org/10.1016/j.molmet.2020.2.005>.
24. Tu H-F, Ko C-J, Lee C-T, Lee C-F, Lan S-W, Lin H-H, Lin H-Y, Ku C-C, Lee D-Y, Chen I-C, Chuang Y-H, Del Caño-Ochoa F, Ramón-Maiques S, Ho C-C, Lee M-S, Chang G-D. Afatinib exerts Immunomodulatory effects by targeting the pyrimidine biosynthesis enzyme CAD. *Cancer Res*. 2021;81(12):3270–82. <https://doi.org/10.1158/0008-5472.CAN-20-3436>.
25. Halbrook CJ, Pontious C, Kovalenko I, Lapienyte L, Dreyer S, Lee H-J, Thurston G, Zhang Y, Lazarus J, Sajjakulnukit P, Hong HS, Kremer DM, Nelson BS, Kemp S, Zhang L, Chang D, Biankin A, Shi J, Frankel TL, Crawford HC, Morton JP, Pasca di Magliano M, Lyssiotis CA. Macrophage-Released pyrimidines inhibit gemcitabine therapy in pancreatic Cancer. *Cell Metab*. 2019;29(6):1390–e13996. <https://doi.org/10.1016/j.cmet.2019.02.001>.
26. Onkar SS, Carleton NM, Lucas PC, Bruno TC, Lee AV, Vignali DAA, Oesterreich S. The great immune escape: Understanding the divergent immune response in breast Cancer subtypes. *Cancer Discov*. 2023;13(1):23–40. <https://doi.org/10.1158/2159-8290.CD-22-0475>.
27. Schmid P, Cortes J, Pusztai L, McArthur H, Kümmel S, Bergh J, Denkert C, Park YH, Hui R, Harbeck N, Takahashi M, Foukakis T, Fasching PA, Cardoso F, Untch M, Jia L, Karantza V, Zhao J, Aktan G, Dent R, O'Shaughnessy J. KEYNOTE-522 investigators. Pembrolizumab for early Triple-Negative breast Cancer. *N Engl J Med*. 2020;382(9):810–21. <https://doi.org/10.1056/NEJMoa1910549>.
28. Sainsbury S, Bernecky C, Cramer P. Structural basis of transcription initiation by RNA polymerase II. *Nat Rev Mol Cell Biol*. 2015;16(3):129–43. <https://doi.org/10.1038/nrm3952>.
29. Moriwaki M, Moore B, Mosbrugger T, Neklason DW, Yandell M, Jorde LB, Welt CK. POLR2C mutations are associated with primary ovarian insufficiency in women. *J Endocr Soc*. 2017;1(3):162–73. <https://doi.org/10.1210/js.2016-1014>.
30. Fang Z-P, Jiang B-G, Zhang F-B, Wang A-D, Ji Y-M, Xu Y-F, Li J-C, Zhou W-P, Zhou W-J, Han H-X. Rpb3 promotes hepatocellular carcinoma through its N-Terminus. *Oncotarget*. 2014;5(19):9256–68. <https://doi.org/10.18632/oncotarget.2389>.
31. Chen X, Zhang N, Zheng Y, Tong Z, Yang T, Kang X, He Y, Dong L. Identification of key genes and pathways in osteosarcoma by bioinformatics analysis. *Comput Math Methods Med*. 2022: 7549894. <https://doi.org/10.1155/2022/7549894>.
32. Zhou D, Li X, Zhao H, Sun B, Liu A, Han X, Cui Z, Yuan L. Combining multi-dimensional data to identify a key signature (Gene and miRNA) of Cisplatin-Resistant gastric Cancer. *J Cell Biochem*. 2018;119(8):6997–7008. <https://doi.org/10.1002/jcb.26908>.

Publisher's note

Springer Nature remains neutral with regard to jurisdictional claims in published maps and institutional affiliations.